Design and Characterization of Geotextiles for High Performance Applications

Sabit Adanur – Textile Engineering, Auburn University
David Elton – Civil Engineering, Auburn University
Tianyi Liao - Post Doctoral Fellow

Goal

To analyze the soil-geotextile interface and develop new geotextile products based on the scientific understanding of this interaction.

Abstract

Substantial amount of work has been done in this project in engineering applications of geotextile. A new computer simulation and analysis method for determining the damage progression and failure strength for nonwoven geotextiles, whose failure mainly is caused by fiber rupture, is presented. The finite element method is used to calculate the numerical solution of stress and strain distribution in different regions of the samples during fabric breaking. Tensile testing is done on several nonwoven fabrics to verify the computer simulated results, which are in good agreement with the experimental results.

1. INTRODUCTION

In recent years the development of new materials and new manufacturing techniques allowed a variety of nonwoven geotextiles to penetrate into high performance areas. These ever-expanding new application areas require textiles to be engineered very carefully and precisely since their failures could have fatal consequences. Our objective is to develop a computer model to analyze the damage progression and failure strength of nonwovens from the knowledge of constituent fibers and the fiber web structure. The characteristics of failure, such as local deformation phenomena, the distribution of the fiber break position and the failure developing trend, will be computed and discussed. Finally, we compare the calculated and experimental results for several nonwovens.

2. NONWOVEN TENSILE FAILURE MODEL

For simulating the nonwoven mechanical behavior in a tensile test, it is necessary to establish a realistic constitutive model which should account for the important features of fabric behavior. In this study, we divide the nonwoven into a network of discrete cell elements for numerical analysis. The properties of the fabric, which is really a continuum, are represented by the mechanical properties of each element. On the other hand, each cell unit represents a finite element for Finite Element Method (FEM). Within each cell unit, fibers in the web are oriented at various directions following random or some known statistical distribution. They are made

up from a number of layers of fibers. In each layer fibers lie in straight lines and are the load carrying elements, offering high stiffness along the length direction. The fiber lateral contraction and compression are negligible. The fiber-fiber interactions within the web, including in bonding, entangling and shear forces, act on the nodal points of the mesh of finite elements. The fibers and filaments that make up the fabric are bound together at the nodal points. Because different sizes and shapes of the finite elements can be adopted according to the specific nonwoven variants, bonding techniques and bonding variants, the distance between the mesh nodal points is adjustable to get a balance between the degree of proper fabric representation desired and the attendant increase in computing time. On the basis of these assumptions, we could deduce the equilibrium equation for each finite element.

In order to simulate the uniaxial tensile experiment, we have chosen the boundary constraint conditions in such a way that one lateral boundary of the sample remains stationary, and the opposite parallel may be displaced by an incremental amount, such as straining the fabric. The amount is set to the value of clamp displacement. The two remaining boundaries are left free to move.

3. EXPERIMENTAL PROCEDURE

Two kinds of nonwovens supplied by the Freudenberg Spunweb Company were used in this study. Fabric A: Lutradure ® 110 TH made from polyester filaments,110 grams per square meter, 0.50 mm thickness under 2KPa. Fabric B: Lutradure ® 210 TH made from polyester filaments, 210 grams per square meter, 0.85 mm thickness under 2KPa. A detailed procedure for obtaining the stress-strain behavior of constituent fibers and the orientation distribution functions were reported in the previous publication.

The tensile properties of the fabrics studied were determined using an Instron tensile testing machine under uniaxial loading of 20.32 cm x 7.62 cm strips at a strain rate of 40 mm/min. At the same time, the entire deformation process of the fabric was recorded by a high resolution video camera and further analyzed using image analysis techniques. A square grid of 7.6 x 7.6 mm was printed on the fabric using black pen, so that the grid marks were clearly visible to the camera when the specimen were under deformation. The main purpose of grid lines were to help with tracing the deformation history.

The recording system consists of a single tube video camera located in front of the mounted specimen ready to be tested on an Instron tensile testing machine. The camera, which can cover an area of 30 cm x 30 cm in the viewing range, was connected to a microcomputer. The image was analyzed on a commercially available image analysis system NIH Image Software. We used the time signature produced by a digital clock in the images to identify images corresponding to the configurations of the specimen under different longitudinal strain levels. The images were captured at 10 second intervals from the beginning of the test to the total rapture of fabric. Since the test was done at a constant strain rate of 40 mm/minute, these time frames corresponded to 3.3%, 6.6%, 9.9%, etc., longitudinal strain levels. The images were then stored in 256 bit gray scale tagged image file format. We then used image enhancement techniques in the system to improve the image quality so as to highlight the fabric features for failure analysis.

4. RESULTS AND DISCUSSION

4.1 Stress-strain Curve

The model fabric for 7.62 cm wide sample was strained in increments of 1% until the last element connecting the two parts separated at a strain of 23%. The stress-strain relations for Fabric A and Fabric B are shown in Fig. 1, where fiber breakage occurs at points denoted by the arrows. Experimental stress-strain curves are also included in the figure. In general, agreement is good between the calculated and experimental curves of the fabric. However, the calculated curves in breaking and rapture parts lie slightly below the experimental ones. In addition, the predicted fabric strength and elongation at the breaking point is insignificantly smaller than the actual data. In the theoretical model, we assumed that the fibers and filaments making up the fabric are bonded together only at nodal points of the finite element. Except the bonding force at nodal points, the acting force between the fibers at other places, such as friction, entangling and cohesive forces, are neglected. This assumption will result in loss of strength and elongation of fabrics at their ultimate failure, which is the reason why the calculated values are smaller than experimental results.

4.2 Development of Fiber Strain

The development trend and procedure of fiber deformations during fabric extension is demonstrated in Fig. 2. The fibers are divided into four categories in terms of their strain level: buckling state, elastic deformation, plastic deformation and failure state.

At the beginning of fabric extension, the number of fibers that suffer compression forces exceed the half of total fibers within the fabric. When the fabric strain is less than 6%, only 37.4% of fibers are extended under elastic deformation. At 7% fabric strain, the forces acting on some fibers are larger than fiber yield stresses, which results in plastic deformation of these fibers. As the fabric strain is increased from 7% to 20%, more and more fibers enter the plastic deformation range. Meanwhile, the percentage of elastically deformed fibers has a general tendency to decrease continually. It is interesting to find some elastic deformed fibers to develop plastic deformation. The number of buckling fibers basically stays constant or lightly increases within this range.

An important point to be considered here is the nature of fiber deformation at 20% fabric strain where fibers begin to rapture. The reason why the fibers, whose breaking elongation is 38%, begin to fail at 20% fabric strain is that the fabric strain and stress values are different in various regions within the sample during extension test. When fabrics are suffered 20% strain, the strains in regions near clamped boundaries and in the center of the sample are much higher than the average value of 20%. In high strain regions, the extension of some fibers exceeds their failure elongation and begin to break. As the deformation proceeds, the number of broken fibers augments significantly. However, the amount of fibers in plastic and elastic deformed states declines sharply. The reason for this is that some fibers start failing as the fabric extension increases. In contrast, more fibers are buckled and compressed . This is the result of fiber rapture in some regions where the fiber loses its resistance to the loading force. The stresses shift to the neighborhood and the stress concentrations occur there. Such stress concentration and redistribution cause more fiber buckling. This certifies that our fiber approach and relaxation techniques used to determine the equilibrium configuration of the strained fabric are feasible and applicable. This strain development mode agrees with the actual situation observed during tensile experiments in normal tensile speed.

Fig. 3 displays the deformation distribution of fibers per 5^0 interval against the orientation angle of fibers with respect to loading direction within the fabric strained at 21%. It is obvious that the broken fibers lay in the loading direction. The fibers parallel to the loading direction rapture first during extension test. The elastically and plastically deformed fibers concentrate in the loading direction, but distribute in a quite wide range. Some asymmetry exists in deformed fiber distribution about the machine direction. In contrast, the buckled fibers are located mainly in the transverse direction. At this strain level, no buckling exists for the fibers oriented in loading direction. 90% of fibers oriented in transverse direction do not carry any load. The fibers lied in longitudinal direction are the main load carriers and play a predominant role on deformation behavior.

Fig. 4 shows the percentages of broken fibers and their locations within the fabric at 20%, 21%, and 22% fabric strain. At 20% fabric strain, the broken fibers are located at two corners of the sample. The breaking develops in a diagonal direction, running from upper left and lower right toward the center of the specimen. At 21% fabric strain the shape of breaking area looks like a diagonal strip across the specimen. As the strain continues, the width of the breaking area spreads out from the diagonal strip toward both sides of the sample. At 22% fabric strain, the elements with the broken fibers nearly link in a row along the width direction of the samples, where the catastrophic failure of the fabric would happen. One interesting discovery we can make from Fig. 5 that, after some fibers break within an element, the rest of the fibers are oriented in other angles within that element and they do not break. The broken fibers do not propagate to cause catastrophic element failure. Nevertheless, the breakage shifts to the neighboring elements. The unbroken fibers in these elements would slip when fabric fails. The number of broken fibers in each element is less than half of the total fibers making up the elements. This shows that the mechanism of nonwoven failure is a combination of fiber breakage and fiber slippage. From Fig. 3, we can see that the broken fibers are mainly oriented in loading direction. This means that during uniaxial tensile extension, the longitudinal fibers located in the diagonal strip of the sample are strained and broken most easily.

4.3 Configuration

Fig. 5 shows the deformed configurations of the specimen at 21%, 22%, and 23% fabric strain which are determined from the models. The experimentally determined configurations of the specimen are also shown in Fig 6. As the fibers are extended to 21% (Fig. 8.a), there is a distortion strip in the diagonal line direction. The area around such distortion is deformed as a result of the slippage, deformation and failures of the fibers in these positions. These areas are designated as the disruption zone. When the failure is loaded up to 22% strain, the disruption zone expands and one side of the sample curls slightly.

At 23% strain, the two parts of the fabric are connected by several elements. The model fabric has essentially failed at this point although these elements remain intact. At that strain value, few elements completely separate the fabric into two disconnected parts. The patterns of fiber failures that lead to fabric failure, which the operator observed during the test, are also indicated in the photographs of Fig. 6. These figures give an indication of how the fabric deform and fail after fiber breakage occurs.

Fig. 7 shows the computed configurations of nonwoven fabric broken in the center and in the side of the specimen near the clamp. The configuration shown in Fig 7.a is very similar to the deformation of fabric observed during tensile testing experiments. In some cases, the actual

deformation shape of nonwoven during Instron tensile tests looks like the graphic shown in Fig. 7.b. This situation happens if the sample is not clamped perfectly in the experiment. Fig. 8 shows the stress distribution within the sample strained into the configurations shown in Fig 7. The stress concentration around the broken area can be seen clearly. The stress and strain in the regions near the broken area and clamp boundaries, particularly in four corners of the sample, are much higher than the other parts of the sample.

5. CONCLUSIONS

Experimental and theoretical computation techniques developed to identify the various changes to fiber web geometry and fiber mechanical behavior that occur during nonwoven deformation and failure are presented. The model can predict not only low strain response but also moderate and high strain response and failure. The local deformation phenomena in a nonwoven fabric subjected to uniaxial tensile loading is investigated. Redistribution of fiber deformation with respect to fiber orientation angles and fiber location within the sample during tensile extension can be examined by a finite element model. The existing standard nonwoven tests can not provide this information, since only the global stress-strain response and failure strength are monitored, and the local mechanisms of fabric deformation and failure are not identified. A good agreement between the experimental results and those from the model, makes it possible to produce optimum nonwoven structures for various applications by selecting the fiber with appropriate properties and designing proper fiber web structure and manufacturing processes.

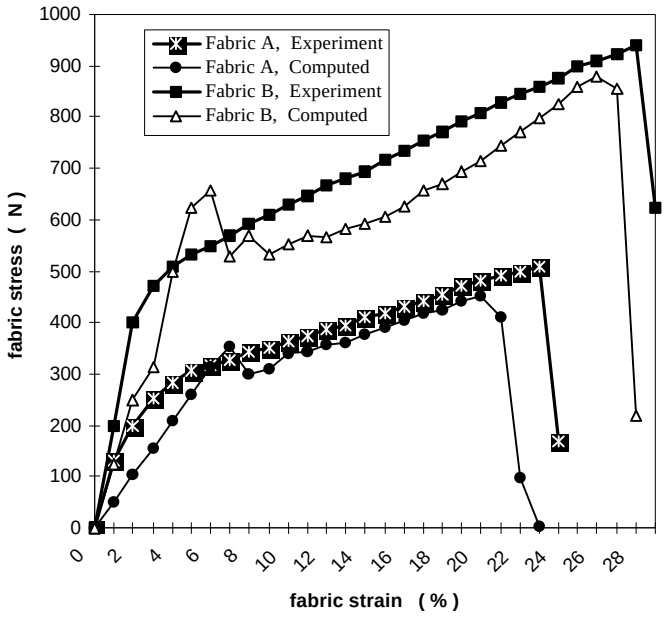

Fig. 1 Experimental stress strain curves and those computed from the models of 7.62cm wide samples

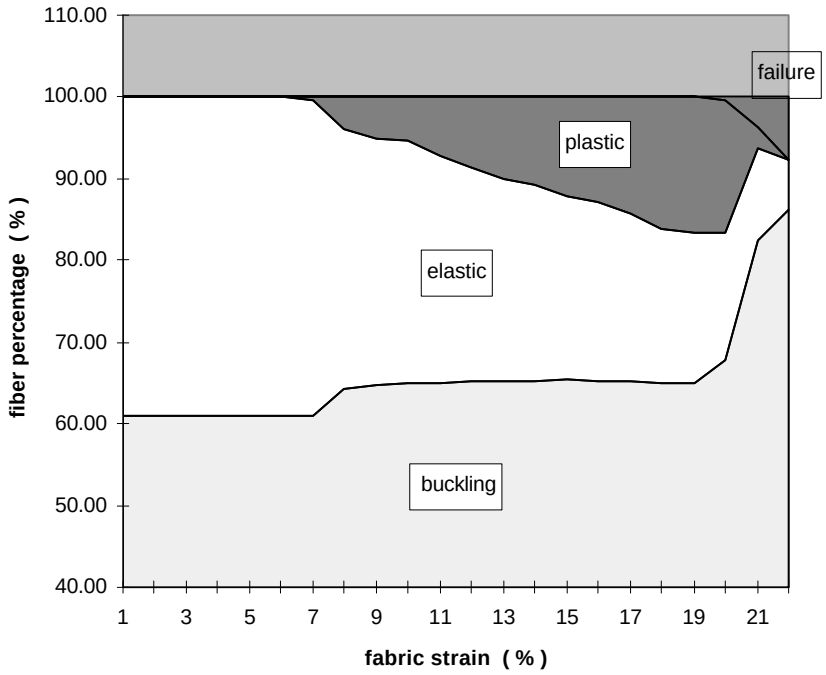

Fig. 2 The interchange progress of fiber deformation states during fabric uniaxial extension.

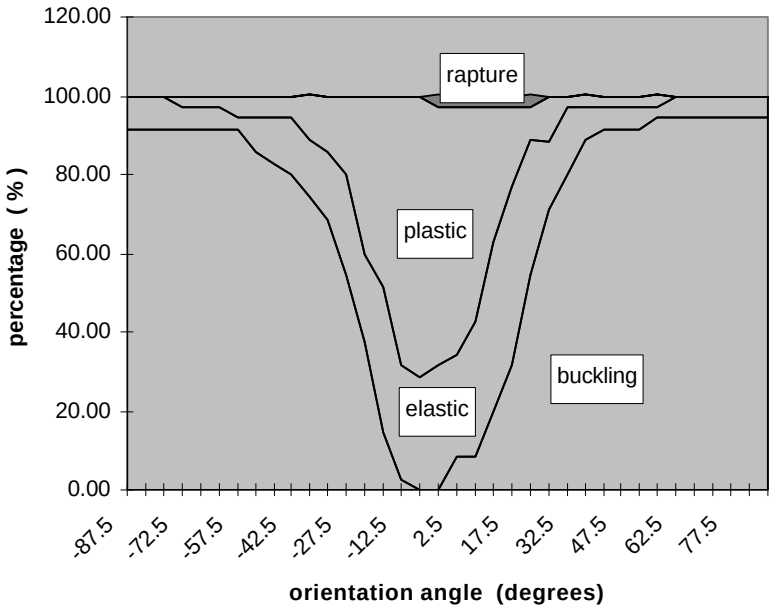

Fig. 3 The deformation distribution of fibers per 50 interval against the orientation angle of fiber with respect to the loading direction when fabric strained 21%.

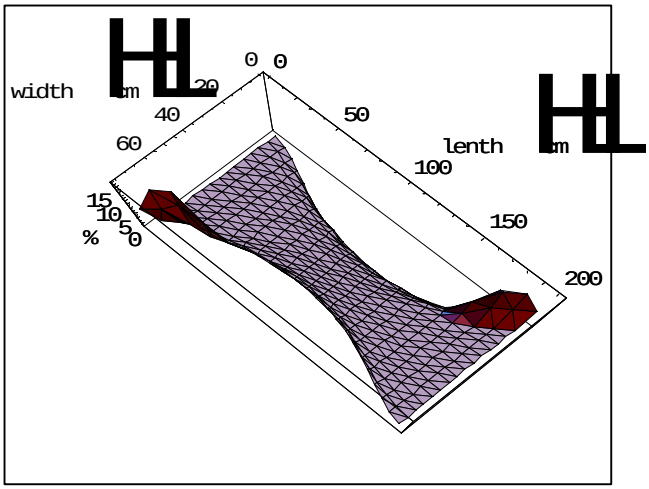

a

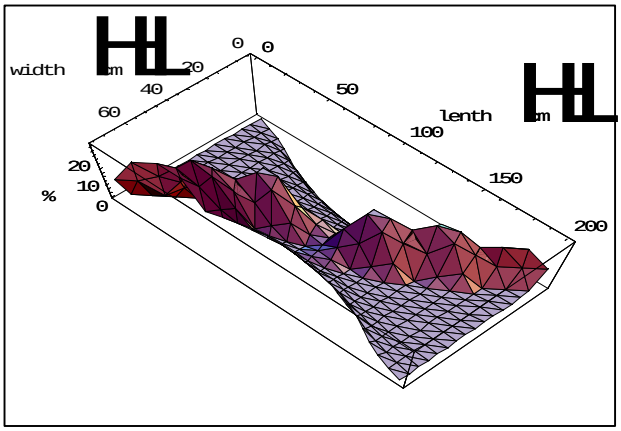

b

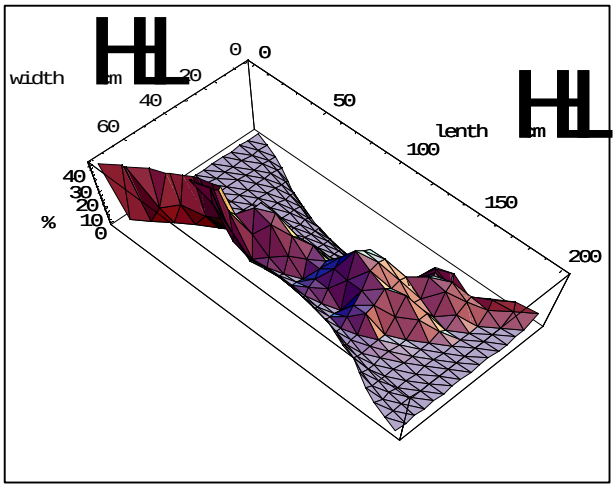

c

Fig. 4 The percentage of broken fibers and their location within the fabric strained at deferent levels before total failure. a, 20%; b, 21%; c, 22%.

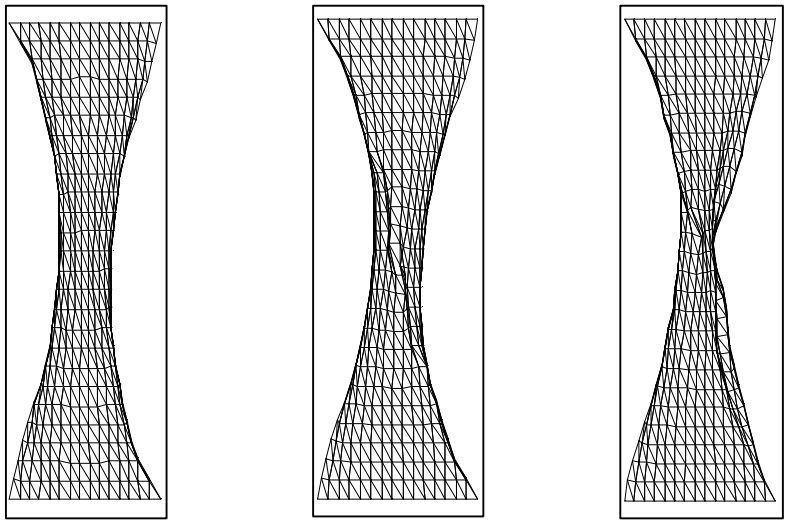

Fig. 5 The computed configurations of Fabric A at 20% (a), 21% (b) and 22% (c) strain during uniaxial extension.

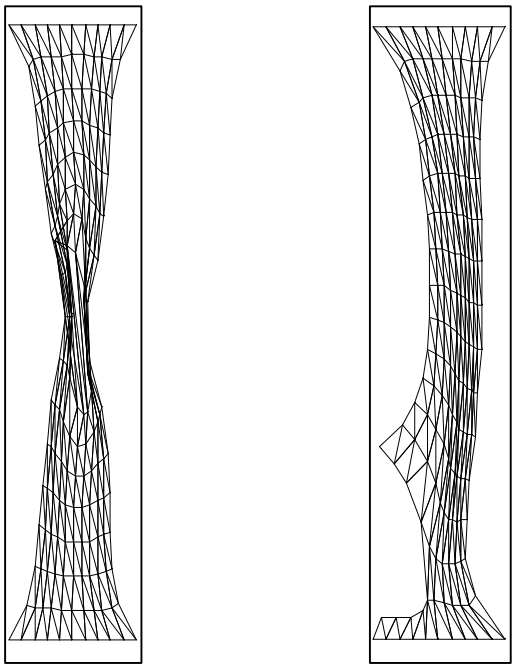

Fig. 7 The computed configurations of geotextile. a: breaking in center; b: breaking near the clamp.

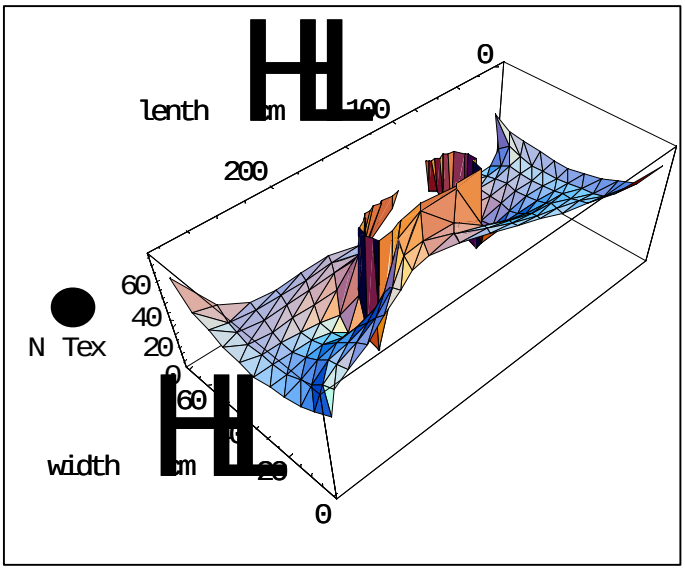

a

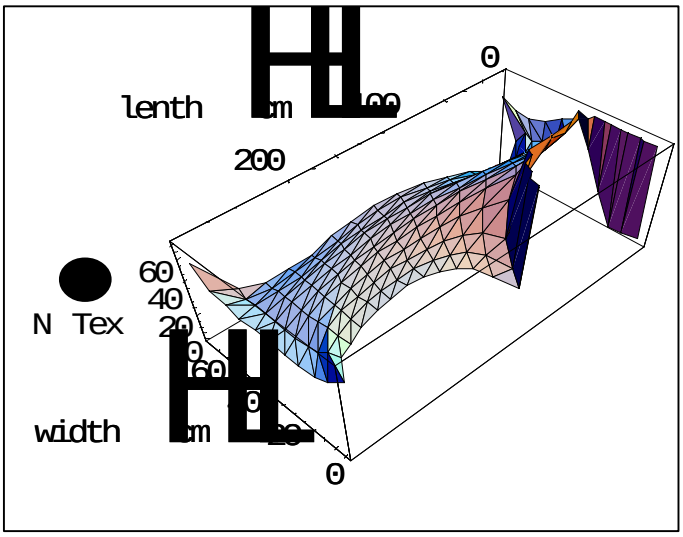

b

Fig. 8 The stress distributions within nonwoven before breaking
a. breaking in center, b. breaking in side near clamp